Evolution of transition-metal-charge states in correlation with the structural and magnetic properties in disordered double perovskites $Ca_{2-x}La_xFeRuO_6$ ($0.5 \leq x \leq 2$)

Kumari Naveen,[1] Tanmay Rom,[1] Shams Sohel Islam,[2] Manfred Reehuis,[3] Peter Adler,[4*] Claudia Felser,[4] Andreas Hoser,[3] Ramesh Chandra Nath,[2] Ashok Kumar Yadav,[5] Shambhu Nath Jha,[5] Dibyendu Bhattacharyya[5] and Avijit Kumar Paul[1*]

[1]*Department of Chemistry, National Institute of Technology Kurukshetra, Kurukshetra-136119, India*

[2]*School of Physics, Indian Institute of Science Education and Research, Thiruvananthapuram-695551, India*

[3]*Helmholtz-Zentrum Berlin für Materialien und Energie, D-14109 Berlin, Germany*

[4]*Max Planck Institute for Chemical Physics of Solids, D-01187 Dresden, Germany*

[5]*Atomic & Molecular Physics Division, Bhabha Atomic Research Centre, Mumbai – 400 094, India*

Keywords: Disordered perovskites; neutron diffraction; crystal structure; antiferromagnetism; oxidation states; resistivity.

Abstract

A series of disordered $Ca_{1.5}La_{0.5}FeRuO_6$, $CaLaFeRuO_6$ and La_2FeRuO_6 double perovskites was prepared by solid-state method and investigated by neutron powder diffraction, x-ray absorption near edge structure (XANES) analysis at the Ru-K edges, Mössbauer spectroscopy, dc magnetization and resistivity measurements. All compounds crystallize in the orthorhombic crystal structure with the space group *Pbnm* down to 3 K showing a random distribution of Fe and Ru at the *B* site. The XANES study reveals a variable Ru^{n+} oxidation state, whereas Mössbauer spectra verify the Fe^{3+} state for all compositions. In $Ca_{1.5}La_{0.5}FeRuO_6$, the majority of Ru ions exist in the +5 oxidation state, whereas $CaLaFeRuO_6$ and La_2FeRuO_6 comprise of mixed oxidation states between +5 and +4 with the highest Ru^{4+} fraction in La_2FeRuO_6. From magnetic susceptibility and neutron diffraction measurements the presence of a *G*-type antiferromagnetic ordering was observed with a drastic increase in transition temperatures from 275 K ($Ca_{1.5}La_{0.5}FeRuO_6$) up to 570 K (La_2FeRuO_6). Mössbauer spectroscopy confirms the presence of long-range ordering but, due to local variations in the exchange interactions, microscopically inhomogeneous magnetic states. All the samples are variable-range-hopping semiconductors. A complex interplay between structural features, charge states, and atomic disorder determines the magnetic properties of the present disordered 3*d*/4*d* double perovskite series.

1. Introduction

Pervoskites show a various range of functional properties due to the strong correlations between charge, spin, lattice and orbital degrees of freedom.[1-5] The presence of unpaired *d* electrons in transition-metal atoms gives rise to several properties such as superconductivity, complex magnetic ordering, large magnetoresistance, ferroelectricity, multiferroicity, thermoelectricity and catalytic activity with great interest in scientific and technical purposes.[6-12] The crystal structures of perovskites with the composition ABO_3 (*B* = transition metals) generally have an arrangement of corner shared BO_6 octahedra. There is a possibility of targeted control of their properties due to chemical flexibility of perovskites to allow a range of structural modifications.[13-15] On one side, the properties of these oxides are strongly influenced by substitution of cations at the *B* site giving mixed valence states as it can be found in double perovskites with the composition $A_2BB'O_6$.[16] On the other hand the *A* site mainly contains divalent cations as Ca^{2+}, Sr^{2+}, Ba^{2+} and/or trivalent rare-earths ions, where size and charge of these cations have a strong influence on structural and physical properties of the perovskite materials.[17-20] The oxidation state of the *B*-site cation is controlled by the average *A*-cationic charge, whereas the size of the *A* cation controls the cooperative tilting of BO_6 octahedra in the perovskite network. The cooperative octahedral tilting affects both the *B*-O bond lengths and *B*-O-*B* bond angles present in perovskites.[21]

The presence of large magnetoresistance in Sr_2FeMoO_6, which belongs to the double perovskite (DP) family, has attracted a great attention for further investigations.[22] Generally, complex properties are found due to competing exchange interactions between the *B* and *B*′ sublattices of DP oxides. These interactions are mainly caused by the presence of two different transition metal cations at the *B* and *B*′ sites and are influenced by their crystallographic arrangement (ordering and disordering).[23-28] Ordering and disordering depend on the size and charge difference between the *B* and *B*′ site transition metal cations. Competing interactions are found between strongly correlated 3*d* and less correlated 4*d* or 5*d* electrons. The additional spin-orbit coupling, present in 4*d*/5*d*-transition elements, is considered to be essential in these interactions. A large number of osmium and iridium based DP's show interesting phenomena due to such coupling.[29-34] Due to the presence of an intermediate spin-orbital-coupling strength and large spatial extent of the charge distribution, 4*d* transition metals, in particular the variable-oxidation state metal Ru, are a good choice for insertion at the *B* site in DP's.[35] In pure Ru perovskites, the rather itinerant 4*d* electrons of Ru give rise to ferromagnetism (FM) in $SrRuO_3$ originating from the low-spin t_{2g}^4-electron configuration of Ru^{4+}, while in case of $Sr_{1-x}Ca_xRuO_3$, an increased isovalent fraction *x*(Ca) leads to a decrease of the CW temperature θ which finally becomes negative, but without leading to long-range antiferromagnetic (AFM) ordering in $CaRuO_3$.[36-37] This shows the loss of long-range ferromagnetic ordering by *A*-site substitution in ruthenates. Interestingly, $LaRuO_3$ containing nominal Ru^{3+} shows metallic character with no long-range magnetic ordering.[38] The coupling between the 4*d* orbital of Ru^{n+} and 2*p* orbital of O^{2-} is responsible for the ferromagnetism in ruthenates and the behaviour can be varied by substitution with magnetic and nonmagnetic ions. Interestingly, a substitution with magnetic ions at the *B* site can give rise to additional magnetic interactions between different magnetic ions creating complex magnetic phase transitions.[39-45]

Although, the *B*-site substitution gives rise to interesting magnetic and electronic properties in DP's, but *A*-site substitution can also lead to peculiar properties, for instance change from long-range ordering to a spin-glass state by Sr^{2+}substitution in the disordered Ca_2FeRuO_6.[46] In case of the $La_{2-x}Sr_xMnRuO_6$ ($0 \leq x \leq 2.0$) system, 50% substitution of Sr^{2+} generates a FM structure, whereas the end member with 100% Sr^{2+} substitution gives rise

to AFM behaviour.[44] In these compounds charge compensation is achieved by changing the valence state of the Mn atoms from 2+ to 4+. This enhances the super-exchange interactions between the Mn^{n+} and Ru^{4+} ions.[47] On the contrary, the oxidation states of both the transition elements change in $La_{1+x}Sr_{1-x}CoRuO_6$ with La^{3+} substitution[48] or in the isovalent substitution series $Ca_{2-x}Sr_xMnRuO_6$.[49] It is well established that ordered DP's reveal a rich variety of magnetic properties which may be useful for device applications, while disordered perovskites can feature unexpected magnetic properties. A recent example is the room temperature ferrimagnetism in Ca_2MnOsO_6.[50] In the present work we have explored the influence of La substitution at the *A* site on the properties of the *G*-type antiferromagnet Ca_2FeRuO_6.[46] Neutron powder diffraction (NPD), magnetization, and transport measurements as well as ^{57}Fe-Mössbauer and x-ray absorption near edge structure (XANES) spectroscopy were applied to unravel the relationship between crystal structure, charge states, and properties in the three *B*-site disordered perovskites $Ca_{1.5}La_{0.5}FeRuO_6$, $CaLaFeRuO_6$, and La_2FeRuO_6. It was found that the magnetic ordering temperature increases drastically from 220 K in Ca_2FeRuO_6 to 570 K in La_2FeRuO_6, whereas on the microscale due to atomic and charge disorder inhomogeneous magnetic states emerge.

2. Experimental details

The conventional solid-state reaction technique was adopted for preparation of $Ca_{1.5}La_{0.5}FeRuO_6$, $CaLaFeRuO_6$ and La_2FeRuO_6 polycrystalline powders by using stoichiometric ratios of binary oxides. Precisely weighed amounts of pure $CaCO_3$/La_2O_3, RuO_2, and Fe_2O_3 (all reagents were almost 99.9% pure and used without further purification) powders with stoichiometric ratios suitable for all compounds were ground in an agate mortar. The powders were pressed into pellets (8 mm diameter and 2 to 3 mm thickness) by using a pressure of 10 bars. The pressed pellets were sintered at 980 and 1280 ^oC (24 h for each temperature) in air with the heating rate of 100^oC/h in each step following intermediate grindings.

Powder *x*-ray diffraction (PXRD) studies were performed using a Rigaku diffractometer with a rotating anode Cu-Kα source. The PXRD patterns were collected from 10 to 80^o in steps of 0.02^o with a counting time of 4 sec per step. Rietveld refinements of the powder diffraction data were carried out with the program *FullProf*. For the x-ray data we used the atomic scattering factors provided by this program. Background refinement is done by using a polynomial function. A pseudo-Voigt function and two asymmetry parameters are used for peak shapes fitting. Neutron powder diffraction experiments of $Ca_{1.5}La_{0.5}FeRuO_6$, $CaLaFeRuO_6$ and La_2FeRuO_6 were carried out on the instruments E6 and E9 at the BER II reactor of the Helmholtz-Zentrum Berlin. The instrument E9 uses a Ge-monochromator selecting the neutron wavelength λ = 1.3087 Å, while the instrument E6 uses a pyrolytic graphite (PG) monochromator selecting the neutron wavelength λ = 2.43 Å. In order to determine in detail the crystal structure parameters at 3 K, powder patterns were recorded on the instrument E9 between the diffraction angles 7.5 and 141.7° (Fig. 1). The magnetic structures of the ruthenates were investigated on the instrument E6, where powder patterns were collected between the diffraction angles from 5.4 to 136.6°. Further, we have followed the temperature dependence of the crystal and magnetic structure on the instrument E6. For the refinements of the neutron powder data the nuclear scattering lengths *b*(O) = 5.805 fm, *b*(Ca) = 4.70 fm, *b*(Fe) = 9.54 fm, *b*(Ru) = 7.03 fm and *b*(La) = 8.24 fm were used.[51-52]

X-ray Absorption Near Edge Structure analysis (XANES) has been carried out at the Ru-K edges to probe the oxidation state of Ru ions. The XANES measurements have been carried out at the Energy-Scanning

EXAFS beamline (BL-9) at the Indus-2 Synchrotron Source (2.5 GeV, 200 mA) at Raja Ramanna Centre for Advanced Technology (RRCAT), Indore, India.[53-54] For the transmission measurement, three ionization chambers (300 mm length each) have been used for data collection, one ionization chamber for measuring the incident flux (I_0), the second one for measuring the transmitted flux (I_t) and the third ionization chamber for measuring the spectrum of a reference metal foil for energy calibration. Appropriate gas pressure and gas mixtures have been chosen to achieve 10-20% absorption in the first ionization chamber and 70-90% absorption in the second ionization chamber to improve the signal to noise ratio.

DC magnetization (M) was measured as a function of temperature (2 K $\leq T \leq$ 850 K) and magnetic field (**–**9 T $\leq H \leq$ +9 T) using the vibrating sample magnetometer (VSM) attachment to the Physical Property Measurement System (PPMS, Quantum Design). For the high temperature ($T \geq$ 400 K) measurements, a high-T oven attachment to VSM was used. The dc resistivity (ρ) was measured as a function of temperature on a small rectangular pellet in the PPMS using the standard four-probe technique.

^{57}Fe-Mössbauer spectra of three compounds were collected from 5.5 up to 315 K using a standard WissEl spectrometer operated in the constant acceleration mode (^{57}Co/Rh source) and a Janis SHI 850-5 closed-cycle refrigerator. The compound powders were mixed with boron nitride and homogeneously distributed in an acrylic glass sample container (~10 mg Fe/cm^2). All isomer shifts are given relative to α iron. The data were evaluated with the MossWinn program using the thin absorber approximation.[55]

3. Results and Discussion

3.1. Crystal Structure

The crystal structures of the mixed series $Ca_{2-x}La_xFeRuO_6$ were investigated by powder *x*-ray diffraction (PXRD) at room temperature and neutron powder diffraction (NPD) at 3 K. Compared to Ca_2FeRuO_6, it was found that the La-containing compounds also crystallize in the orthorhombic structure with the space group *Pbnm* which verifies the random ordering of Fe and Ru atoms at the octahedral *B* site in the present perovskites. Further, no additional peak splitting could be observed indicating the absence of a lower symmetric monoclinic structure. Both, Fe and Ru atoms statistically occupy the Wyckoff position 4*b*(½,0,0). The Ca and O1 atoms are located at the Wyckoff position 4*c*(*x*,*y*,¼), while the O2 atoms are located at the position 8*d*(*x*,*y*,*z*). The shifting of the diffraction peaks to lower scattering angles from $Ca_{1.5}La_{0.5}FeRuO_6$ to La_2FeRuO_6 reflects the successive Ca^{2+} substitution by the larger La^{3+}ions. It is resulted the continuous increase of the lattice parameters and the cell volume (Fig. 2). The crystal structure parameters were refined by Rietveld analysis using NPD data collected at 3 K as shown in Fig. 1. All refined structural parameters and residuals R_F are listed in Table 1. The average bond length d_{av}(*B*-O) in the BO_6 octahedra, where the Fe and Ru atoms are statistically distributed, shows a significant increase from 1.972(2) to 2.018(11) Å if Ca is replaced by La (Fig. 2). Further it is pointed out that the averaged bond angle ∠(*B*-O-*B*) is increasing form 152.4(2) to 156.4(3)° with increasing La content which may influence the strength of the exchange interactions and thus for the magnetic properties.

The chemical formula of the end members of the system $Ca_{2-x}La_xFeRuO_6$ can be given in detail as $Ca_2^{4+}[Fe^{3+}Ru^{5+}O_6^{12-}]^{4-}$ and $La_2^{6+}[Fe^{3+}Ru^{3+}O_6^{12-}]^{6-}$.[56] Our Mössbauer measurements (described below) confirmed that the charge of the iron ions remains 3+ for all the studied compounds. Accordingly, an ionic radius $r(Fe^{3+})$ =

0.615 Å and a typical bond length $d(Fe^{3+}\text{-}O^{2-})$ = 2.015 Å is expected and it can be concluded that only the charge of ruthenium is changing, which is finally the cause of the increase in bond distance by $\Delta d_{av}(B\text{-O})$ = 0.050 Å. Using the ionic radii given by Shannon [$d(Ru^{3+})$ = 0.68 Å, $d(Ru^{4+})$ = 0.62 Å, $d(Ru^{5+})$ = 0.565 Å, $d(O^{2-})$ = 1.40 Å] the expected bond lengths are the following: $d(Ru^{3+}\text{-}O^{2-})$ = 2.08 Å, $d(Ru^{4+}\text{-}O^{2-})$ = 2.02 Å, and $d(Ru^{5+}\text{-}O^{2-})$ = 1.965 Å.[57] Then the averaged expected bond lengths are $d(Fe^{3+}/Ru^{3+}\text{-}O^{2-})$ = 2.048 Å, $d(Fe^{3+}/Ru^{4+}\text{-}O^{2-})$ = 2.018 Å, and $d(Fe^{3+}/Ru^{5+}\text{-}O^{2-})$ = 1.990 Å. For Ca_2FeRuO_6 the determined $d_{av}(T\text{-O})$ = 1.980(9) Å is close to the expected averaged value $d(Fe^{3+}/Ru^{5+}\text{-}O^{2-})$ = 1.990Å. This clearly indicates that ruthenium exists in Ca_2FeRuO_6 as Ru^{5+}. As already mentioned above, for stoichiometric La_2FeRuO_6 it is expected that ruthenium exists as Ru^{3+}. However, the observed bond distance $d(B\text{-}O^{2-})$ = 2.018 Å is somewhat smaller than the expected value $d(Fe^{3+}/Ru^{3+}\text{-}O^{2-})$ = 2.048 Å, and is in perfect agreement with $d(Ru^{4+}\text{-}O^{2-})$ = 2.018 Å. A predominant Ru^{4+} oxidation state in La_2FeRuO_6 is also consistent with our XANES study (shown later). This suggests that the charge balance rather may involve creation of cation vacancies. In fact, samples of La_2FeRuO_6 which were synthesized earlier by heating in Ar or N_2 atmosphere, were found to be non-stoichiometric having the compositions as $La_2FeRuO_{6.30}$ and $La_2FeRuO_{6.12}$, respectively.[56] It was pointed out that the perovskite structure cannot accept excess oxygen and thus rather cation vacancies, possibly mainly on the La sites, are created. Accordingly, we tried to refine the La occupancies within the Rietveld analysis of the NPD data, but were unable to verify a significant La deficiency in La_2FeRuO_6. In our crystal structure refinements the ratio *occ*(La)/*occ*(O) reaches practically a value of 2. The present sample was prepared by annealing in air and thus, the average Ru oxidation state should be even higher than the Ru oxidation states for the earlier reported samples.[56] This is in agreement with the smaller unit cell volume of the present samples compared to the volumes of the previous samples (245.24 $Å^3$ vs 246.97 $Å^3$). Mixed cation deficiency on both, the La and Ru sites was reported for the nominal Ru^{3+} perovskite $LaRuO_3$ which was prepared in N_2 atmosphere.[57] In the present materials, the simultaneous presence of cation disorder and possible non-stoichiometry at both the La and the transition metal sites may render an unambiguous determination of their composition from the NPD difficult.

3.2. X-ray Absorption Spectroscopy

X-ray Absorption Spectroscopy (XAS) measurements, comprising of both X-ray Absorption Near Edge Structure (XANES) and Extended X-ray Absorption Fine Structure (EXAFS) techniques, have been carried out at room temperature in transmission mode at Ru-K edge to derive the Ru-oxidation states and to unravel the local structure. The oxidation state of Ru is calculated using the empirical method described by Vitova et al. for Ru based perovskites.[58] The peak position in the derivative spectrum (Fig. 3) is obtained from Gaussian fits to the experimental curve. A linear fit is performed for correlating the oxidation states of reference samples and energy shifts (ΔE) with respect to metallic Ru (Fig. 4). Using a linear function between the oxidation state and the shift of the Ru-K edge (ΔE), the mean oxidation state n of Ru^{n+} was calculated for the three $Ca_{2-x}La_xFeRuO_6$ compounds studied here and summarized in Table 2. It is obvious that the mean oxidation state of Ru decreases with increasing La content, but for La_2FeRuO_6 it is much larger than the nominal value of +3 expected for stoichiometric La_2FeRuO_6. The reference compounds used for the analysis include metals as well as insulators. Referring to Fig. 4(b) it is seen that the oxidation states of the insulators $RuCl_3$ and Ca_2FeRuO_6 having well-defined oxidation states of +3 and +5, respectively, are somewhat underestimated by the linear function. This suggests that also the values

of the oxidation state of the $Ca_{1.5}La_{0.5}FeRuO6$ may also be enhanced by about 0.2. In any case it is evident that the difference between the expected Ru oxidation states for the stoichiometric compound and that of the actual compound increases with increasing La content which suggests an increasing degree of non-stoichiometry or the presence of small impurity of amorphous La_2O_3.[56]

The local structure around the absorbing atom is obtained from the quantitative analysis of EXAFS spectra.[59] The Fourier transform EXAFS spectra [$\chi(R)$ vs R] at the Ru-K edge are shown in Fig. 5 along with best fitting results. The fitting is carried out for first coordination shell using a single Ru-O scattering path. The bond lengths R, coordination number N and disorder factor (σ^2) are used as fitting parameters. The fitting results are shown in Table 3. Fig. 5 shows the enlarged portion of the first coordination peak at ~1.5 Å. The position of the peak is indicative for bond length and the amplitude of the peak is related with oxygen coordination number in the first coordination shell. The maximum amplitude is obtained for Ca_2FeRuO_6 at relatively lower distance, however the minimum peak amplitude is observed for La_2FeRuO_6 at relatively larger distance. The bond lengths obtained from the fittings (Table 3) are in good agreement with those obtained from XRD while the coordination numbers show large errors. A decreased N for the compounds with large La contents could suggest oxygen deficiency which is, however, not confirmed by the neutron data.

3.3. DC Magnetization

The temperature dependent molar magnetic susceptibility $\chi_m(T)$ curves for all compounds were calculated assuming nominal stoichiometries and are shown in Fig. 6. Zero-field cooled (ZFC) and field-cooled (FC) curves show a clear divergence for $Ca_{1.5}La_{0.5}FeRuO_6$ and $CaLaFeRuO_6$ in the temperature range from 250 to 300 K. The ZFC and FC curves have similar shapes for the two compounds, with a maximum at a certain temperature $T_{m'}$ in the ZFC curve and strong increase below ~250 K in the FC curves. For La_2FeRuO_6, there is no deviation between ZFC and FC curves and a broad hump is present in both curves at around 320 K indicating long-range antiferromagnetic ordering. In all the compounds, iron is expected to be in the ionic state of Fe^{3+} (d^5; S = 5/2), but the average Ru-oxidation states decreases in the series as suggested by the structural and XANES data. The inverse susceptibility curves $\chi_m^{-1}(T)$ show curvature over extended temperature ranges. The combined neutron and Mössbauer studies described below suggest that the susceptibility curves reflect an inhomogeneous magnetic behavior where magnetic correlations persist up to high temperatures. Therefore, Curie-Weiss analysis of the data is not meaningful. The statistic mixture of Ca-La and of Fe-Ru ions together with non-stoichiometry effects induces a complicated balance of superexchange interactions which also may generate weak ferromagnetic interactions.[60] Note that the magnetic properties of the present La_2ReRuO_6 sample differ completely from those of previous materials which were prepared under reducing conditions and reported to be spin glasses.[56]

In order to further characterize the nature of the magnetic states, magnetic isotherm (M vs H) data were measured at different temperatures (Fig. 7). The linear magnetization curves above room temperature for all compounds are indicating either the paramagnetic regime or antiferromagnetic order. In $Ca_{1.5}La_{0.5}FeRuO_6$ and $CaLaFeRuO_6$, the presence of hysteresis loops at lower temperatures suggests weak ferromagnetic components in the magnetic response of both compounds, but without any saturation up to 9 T. Considering that the Mössbauer spectra (see below) evidence magnetic order at room temperature it is concluded that La_2FeRuO_6 is AFM due to the presence of a linear magnetization curve up to 380 K. The weak ferromagnetic components in $Ca_{1.5}La_{0.5}FeRuO_6$ and $CaLaFeRuO_6$ give rise to small remanent magnetization values of 0.026 μ_B and 0.031 μ_B for

$Ca_{1.5}La_{0.5}FeRuO_6$ and $CaLaFeRuO_6$, respectively. Incomplete compensation of moments and/or spin canting may be the origin for this observation.

3.4. Magnetic Structure

In order to investigate the magnetic order of $Ca_{1.5}La_{0.5}FeRuO_6$, $CaLaFeRuO_6$ and La_2FeRuO_6, we have collected neutron powder patterns on the instrument E6 from 3 to 570 K. As found earlier for Ca_2FeRuO_6 the strongest magnetic intensity was observed at the position of the reflection pair 101/011 (Fig. 8). For the Fe and Ru atoms in the position 4*b*(½,0,0; ½,0,½; 0,½,0; 0,½,0) magnetic intensity could be generated with a *G*-type model, where the spin sequence is + − − +. We have shown previously that the magnetic moments in Ca_2FeRuO_6 are aligned parallel to the *c* axis.[46] The same type of ordering was found for the present compounds $Ca_{1.5}La_{0.5}FeRuO_6$, $CaLaFeRuO_6$ and La_2FeRuO_6, but for the compound with higher La content it was difficult to determine precisely the moment direction due to the reduction of the lattice distortions. In Fig. 2 it is seen that the *b* parameter is somewhat larger than *a* and $c/\sqrt{2}$. This allowed us to exclude a magnetic ordering, where the moments are aligned parallel to the *b* axis. On the other hand, the instrumental resolution is not sufficient to distinguish between a moment direction parallel *a* or *c*. But due to the fact that the magnetic patterns of all compounds are very similar we assumed that the moments are aligned parallel to the *c* axis. With this model the magnetic moments were determined by Rietveld refinements resulting in satisfactory residuals (defined as $R_M = \sum||I_{obs}| - |I_{calc}||/\sum|I_{obs}|$) between 0.047 and 0.055. From the data sets collected at 3 K the following magnetic moments have been determined: μ_{exp} = 2.25(3) μ_B ($Ca_{1.5}La_{0.5}FeRuO_6$), μ_{exp} = 2.41(3) μ_B ($CaLaFeRuO_6$), μ_{exp} = 2.74(3) μ_B (La_2FeRuO_6). Here it is interesting to see that the ordered magnetic moment at the Fe/Ru site seems to become larger with increasing La content. But on the other hand, the end member Ca_2FeRuO_6 reaches a moment μ_{exp} = 2.66(2) μ_B, which is similar to the value of the other end member La_2FeRuO_6. This shows that there is no systematic change in the moments, despite the fact that the charge of the ruthenium ions changes from +5 to a value of about +4. Further, the reduced moment of the Ca-La mixed compounds may be ascribed to their stronger disordered character. In the next step we tried to estimate the magnetic moment of the Ru^{n+} ions. For the free Fe^{3+} ion, which is in the d^5 state, a theoretical magnetic moment of 5.0 μ_B is expected. On the other hand, it is known for other ternary iron oxides that the experimental magnetic moment of the Fe^{3+} ion is found to be considerably reduced: μ_{exp} = 3.55(5) μ_B in $Sr_4Fe_4O_{11}$, μ_{exp} = 3.5(1) μ_B in $CaFeO_3$, and μ_{exp} = 3.34(7) μ_B in Sr_2FeOsO_6.[31, 61-65] Thus for the system $Ca_xLa_{2-x}FeRuO_6$, one can expect for the Fe^{3+} ion a moment of $\mu_{exp} = 3.5\mu_B$. Due to the fact that the occupancy of Fe on the *B* site is 0.5 one obtains a moment of $1.75\mu_B$ due to Fe^{3+}. Therefore, it can be estimated that the Ru^{n+} ions carry a moment of about 1 μ_B.

The temperature dependence of the magnetic moment of $Ca_{1.5}La_{0.5}FeRuO_6$, $CaLaFeRuO_6$, and La_2FeRuO_6 is shown in Fig. 9. Long-range magnetic ordering sets in at 275 K ($Ca_{1.5}La_{0.5}FeRuO_6$), 435 K ($CaLaFeRuO_6$), and 570 K (La_2FeRuO_6), respectively. The increase in the ordering temperature can be partly attributed to a decrease in the structural distortion (increasing average *B*-O-*B* angle) and a concomitant strengthening of the Fe/Ru-O-Fe/Ru exchange interactions with increasing La content. On the other hand, the average Ru-charge state is changed within the series and it is likely that the complex balance of exchange interactions in the disordered DP's [16, 46] is varied due to the replacement of Ru^{5+} (t_{2g}^3) by Ru^{4+} (t_{2g}^4) or Ru^{3+} (t_{2g}^5) ions. This clue is consistent with the corresponding decrease of the ferromagnetic component in the *M*(*H*) data, which vanishes in La_2FeRuO_6 (Fig. 7). Together with the high ordering temperature this may indicate the

dominance of the strong AFM interactions between the Fe^{3+} ($t_{2g}^3 e_g^2$) ions in La_2FeRuO_6. The $m(T)$ curves are quite gradual showing an inflection for x = 0.5 and 2.0 and a plateau for x = 1 which indicates an inhomogeneous magnetic state on the microscale, in agreement with the Mössbauer studies described in the following.

3.5. Mössbauer Spectroscopy

Mössbauer spectra of the $Ca_{2-x}La_xFeRuO_6$ compounds with x = 0.5, 1, and 2 are shown in Fig. 10. Similar as for Ca_2FeRuO_6,[46] the spectra show broad magnetic hyperfine patterns which are typical for inhomogeneous magnetic systems. The magnetic hyperfine patterns were described by hyperfine field (B_{hf}) distributions which were extracted according to the model-independent Hesse-Rübartsch method. Most remarkably, the low-temperature spectra show very similar hyperfine patterns for all three compounds with an identical isomer shift of 0.49 mm/s and hyperfine fields around 50 T. The spectra demonstrate unambiguously that the Fe ions are in the +3 high-spin states in all these compounds which are in agreement with previous room temperature Mössbauer spectra[65] and verifies that any valence changes due to substitution of Ca^{2+} by La^{3+} ions must be associated with the Ru ions. This is in contrast to manganese-based disordered DP's $Ca_{2-x}Sr_xMnRuO_6$[49] where mixed valency occurs on both transition metal sites. For all three compounds the Fe moments are fully ordered at base temperature (~ 5 K). The peak hyperfine field of the B_{hf} distribution increases continuously with increasing La content from 48 T for x = 0 to 53 T for x = 2, suggesting that the local moments at the Fe sites slightly increase with the La content. The spectra of the compounds with x = 0.5 and 1 show a partial collapse of the hyperfine patterns between 100 and 150 K and between 150 and 200 K, respectively, and somewhat broadened quadrupole doublets appeared inthe spectra at $T \geq 150$ K for x = 0.5 and $T \geq 200$ K for x = 1, indicating that the compounds partly have transformed to the paramagnetic state. Accordingly, the maxima in the respective ZFC magnetic susceptibility curves at $T_{m'}$ =120 and 170 K (Fig. 6) can be assigned to antiferromagnetic ordering of a significant fraction of the iron sites (doublet area fractions of ~43% for x = 0.5 at 150 K and ~55% for x = 1 at 200 K). However, the transition to the paramagnetic state is not complete above $T_{m'}$ and broad magnetic hyperfine structures are superimposed to the quadrupole doublets even in the spectra at 250 and 290 K for x = 0.5 and 1, respectively. These results compare well with the neutron diffraction data which still show magnetic Bragg reflections in this temperature range and indicate that the magnetic ordering vanishes completely near 275 K for x = 0.5 and 435 K for x = 1. Both, the neutron diffraction and the Mössbauer data show that there is no sharp magnetic ordering transition, but a sluggish loss of magnetic ordering. The magnetic inhomogeneity is the consequence of the variation in the local environment of the magnetic ions and thus in the exchange interactions which also explains the absence of a clear feature in the magnetic susceptibility data reflecting well-defined onset of magnetic ordering. Thus, the Mössbauer spectra show that the magnetic ordering process extends over a broad temperature range. A major fraction of the compound ordersin a relatively narrow temperature range below 150 and 200 K for x = 0.5 and 1, respectively, whereas the remaining part orders at higher temperatures.

A similar behavior, albeit at considerably higher temperatures, is found for La_2FeRuO_6. The magnetic susceptibility curve shows a maximum near 300 K. The Mössbauer spectra reveal that the majority of the compound is still magnetically ordered at 315 K but a sharp feature in the center of the spectrum indicates an inward collapse which suggests that part of the compound approaches already the paramagnetic state. Such a feature is already discernible in the 200 K spectra. All together these data show that due to Fe-Ru disorder and

variation in Ru charge, the magnetic state in La_2FeRuO_6 is very inhomogeneous with a broad distribution of ordering temperatures.

3.6. Transport Properties

The temperature dependent electrical resistivity $\rho(T)$ measurements were performed at zero field by adopting the conventional four-probe method. The ρ vs T curves for all the three compounds are shown in the upper panel of Fig. 11. With decreasing temperature all the three compounds show a rapid increase in ρ, suggesting that the ground state is insulating in nature. Below 50 K, ρ (T) exceeded the measurable limit of the instrument and hence could not be measured. To extract the activation energy, the temperature dependent conductivity ($\sigma = 1/\rho$) data were fitted by the Arrhenius transport relation

$$\sigma = \sigma_0 \exp(-\Delta/k_B T). \qquad (3)$$

Here, σ_0 is the proportionality constant, Δ is the activation energy, and k_B is the Boltzmann constant. In the inset of the upper panel of Fig. 11, ln σ vs $1/T$ is plotted. It shows a nearly linear behaviour in the high temperature region and deviates significantly from linearity at low temperatures. A straight line fit in the high temperature range regime 200 K ≤ T ≤ 300 K, 170 K ≤ T ≤ 300 K, and 178 K ≤ T ≤ 300 K for La_2FeRuO_6, $CaLaFeRuO_6$, and $Ca_{1.5}La_{0.5}FeRuO_6$ yields $\Delta \simeq 0.15$ eV, 0.11 eV, and 0.09 eV, respectively. The increase in activation energy from 0.09 to 0.15 eV indicates that La doping at the Ca site effectively enhances the band gap, thereby decreasing the conductivity.

It is generally observed that in real materials, the simple Arrhenius equation is not adequate to describe the transport properties at low temperatures. According to Mott and Davis, the low-temperature transport can be described by the three-dimensional variable range hopping (VRH) mechanism which can be defined by the equation (4)

$$\sigma(T) = \sigma_1 \exp[-(T_0/T)^{1/4}] \qquad (4)$$

Here, σ_1 and T_0 are constants. T_0 can be written as $T_0 = 24/[\pi k_B N(E_F)\xi^3]$, where $N(E_F)$ is the density of states at the Fermi level and ξ is the decay length of the localized spin wave function. As shown in the lower panel of Fig. 9, our ln σ vs $T^{-1/4}$ plots for all three compounds show almost linear behaviour over the whole measured temperature range. The corresponding straight line fit resulted $\sigma_1 \simeq 8.3\times10^{10}$ Scm^{-1} and $T_0 \simeq 1.5\times10^8$ K for La_2FeRuO_6, $\sigma_1 \simeq 1.23\times10^{11}$ Scm^{-1} and $T_0 \simeq 8.4\times10^7$ K for $CaLaFeRuO_6$, and $\sigma_1 \simeq 5.25\times10^9$ $Scm^{-1}$and $T_0 \simeq 5.1\times10^7$ K for $Ca_{1.5}La_{0.5}FeRuO_6$. This clearly supports the fact that at low temperatures, conduction is taking place by a hopping mechanism in the vicinity of the Fermi energy. Evidence of VRH mechanism was also found previously in several other double-perovskite materials.[29, 66-68]

4. Conclusions

The structural, magnetic, and transport properties of three disordered La-based double perovskites of the system $Ca_{2-x}La_xFeRuO_6$ ($0.5 \le x \le 2$) were thoroughly investigated by several techniques. The crystal structures are found to have orthorhombic symmetry with the space group *Pbnm*. All the compounds are atomically disordered at the *B*-site and magnetically ordered. Mössbauer spectra show that Fe is always in 3+ oxidation state, whereas XANES data evidence that the Ru ions are present in mixed $Ru^{3+}/Ru^{4+}/Ru^{5+}$ oxidation states. The highest Ru^{4+} fraction is found for La_2FeRuO_6, but there is no evidence for Ru^{3+} expected for stoichiometric La_2FeRuO_6,

which suggests the presence of cation vacancies. The analysis of the neutron diffraction data reveals that the investigated double perovskites show an antiferromagnetic *G*-type ordering, and Mössbauer spectroscopy reveals large microscale inhomogeneity of the magnetic states reflecting local variations in the exchange interactions. An increasing degree of La substitution leads to a drastic increase in the magnetic ordering temperature from 220 K in Ca_2FeRuO_6 to 570 K in La_2FeRuO_6. The complex balance of superexchange interactions between the magnetic *B* ions is altered in these disordered DP's due to the structural and Ru valence changes caused by the substitution of Ca^{2+} by larger La^{3+} cations at the *A* site. Resistivity data show that with increasing La content, the activation energy for the electron transport increases and suggest a variable range hopping transport mechanism. The present system is an example for the realization of high magnetic ordering temperatures in atomically disordered 3*d*/4*d* double perovskites.

Acknowledgements

Authors acknowledge the Department of Science and Technology for the financial support through INSPIRE Award (No. IFA14-CH-144), India. This research was supported in part by SERB, India (No. SB/FT/CS-098/2014).

Corresponding Authors

*Email: [1]apaul@nitkkr.ac.in

[3]adler@cpfs.mpg.de

References

[1] R. Morrow, A. E. Taylor, D. J. Singh, J. Xiong, S. Rodan, A. U. B. Wolter, S. Wurmehl, B. Büchner, M. B. Stone, A. I. Kolesnikov, A. A. Aczel, A. D. Christianson and P. M. Woodward, Spin-orbit coupling control of anisotropy, ground state and frustration in 5*d*^{2} Sr_2MgOsO_6, *Sci. Rep*., 2016, **6**, 32462.

[2] A. E. Taylor, R. Morrow, R. S. Fishman, S. Calder, A. I. Kolesnikov, M. D. Lumsden, P. M. Woodward and A. D. Christianson, Spin-orbit coupling controlled ground state in Sr_2ScOsO_6, *Phys. Rev. B*, 2016, **93**, 220408(R).

[3] X. Wang, M. Liu, X. Shen, Z. Liu, Z. Hu, K. Chen, P. Ohresser, L. Nataf, F. Baudelet, H.-J. Lin, C.-T. Chen, Y.-L. Soo, Y.-F. Yang, C. Jin and Y. Long, High-temperature ferromagnetic half metallicity with wide spin-up energy gap in $NaCu_3Fe_2Os_2O_{12}$, *Inorg. Chem.*, 2019, **58**, 320.

[4] M. Liu, C.-E Hu, and X.-R. Chen, Electronic and magnetic properties of 5*d*^{1}, 5*d*^{2} and 5*d*^{3}double perovskites Ba_2MOsO_6 (*M* = K, Ca, and Sc): Ab initio study, *Inorg. Chem.*, 2018, **57**, 444.

[5] C. A. Marjerrison, C. M. Thompson, G. Sala, D. D. Maharaj, E. Kermarrec, Y. Cai, A. M. Hallas, M. N. Wilson, T. J. S. Munsie, G. E. Granroth, R. Flacau, J. E. Greedan, B. D. Gaulin and G. M. Luke, Cubic Re^{6+} (5*d*^{1}) Double perovskites, Ba_2MgReO_6, Ba_2ZnReO_6, and $Ba_2Y_{2/3}ReO_6$: Magnetism, heat capacity, μSR, and neutron scattering studies and comparison with theory, *Inorg. Chem.*, 2016, **55**, 10701.

[6] Y. Inaguma, A. Aimi, D. Mori, T. Katsumata, M. Ohtake, M. Nakayama and M. Yonemura, High-pressure synthesis, crystal structure, chemical bonding, and ferroelectricity of $LiNbO_3$-Type $LiSbO_3$, *Inorg. Chem.*, 2018, **57**, 15462.

[7] H. L. Feng, Z. Deng, M. Wu, M. Croft, S. H. Lapidus, S. Liu, T. A. Tyson, B. D. Ravel, N. F. Quackenbush, C. E. Frank, C. Jin, M.-R. Li, D. Walker and M. Greenblatt, High-pressure synthesis of Lu_2NiIrO_6 with ferrimagnetism and large coercivity, *Inorg. Chem.*, 2019, **58**, 397.

[8] H. L. Feng, M. Reehuis, P. Adler, Z. Hu, M. Nicklas, A. Hoser, S.-C. Weng, C. Felser and M. Jansen, Canted ferrimagnetism and giant coercivity in the nonstoichiometric double perovskite $La_2Ni_{1.19}Os_{0.81}O_6$, *Phys. Rev. B*, 2018, **97**, 184407.

[9] H. L. Feng, P. Adler, M. Reehuis, W. Schnelle, P. Pattison, A. Hoser, C. Felser and M. Jansen, High-temperature ferrimagnetism with large coercivity and exchange bias in the partially ordered 3*d*/5*d* hexagonal perovskite $Ba_2Fe_{1.12}Os_{0.88}O_6$, *Chem. Mater.*, 2017, **29**, 886.

[10] Q. Sun, and W.-J. Yin, Thermodynamic stability trend of cubic perovskites, *J. Am. Chem. Soc.*, 2017, **139**, 14905.

[11] S. T. Hartman, S. B. Cho and R. Mishra, Multiferroism in iron-based oxyfluoride perovskites, *Inorg. Chem.*, 2018, **57**, 10616.

[12] B. Han, A. Grimaud, L. Giordano, W. T. Hong, O. Diaz-Morales, Y.-L. Lee, J. Hwang, N. Charles, K. A. Stoerzinger, W. Yang, M. T.M. Koper and Y. Shao-Horn, Iron-based perovskites for catalyzing oxygen evolution reaction, *J. Phys. Chem. C*, 2018, **122**, 8445.

[13] G. Volonakis, N. Sakai, H. J. Snaith and F. Giustino,Oxide Analogs of Halide Perovskites and the New Semiconductor Ba_2AgIO_6, *J. Phys. Chem. Lett.*, 2019, **10**, 1722.

[14] C. J. Bartel, C. Sutton, B. R. Goldsmith, R. Ouyang, C. B. Musgrave, L. M. Ghiringhelli and M. Scheffler, New tolerance factor to predict the stability of perovskite oxides and halides, *Mater. Sci*., 2019, **5**, eaav0693.

[15] J. E. Page, H. W. T. Morgan, D. Zeng, P. Manuel, J. E. McGrady andM. A. Hayward, Sr_2FeIrO_4: Square-planar Ir(II) in an extended oxide, *Inorg. Chem.*, 2018, **57**, 13577.

[16] S. Vasala and M. Karppinen, $A_2B'B''O_6$ perovskites: A review, *Prog. Solid State Chem.*, 2015, **43**, 1-36.

[17] A. K. Paul, A. Sarapulova, P. Adler, M. Reehuis, S. Kanungo, D. Mikhailova, W. Schnelle, Z. Hu, C. Kuo, V. Siruguri, S. Rayaprol, Y. Soo, B. Yan, C. Felser, L. H. Tjeng and M. Jansen, Magnetically frustrated double perovskites: Synthesis, structural properties, and magnetic order of Sr_2BOsO_6 (B = Y, In, Sc), *Z. Anorg. Allg. Chem.*, 2015, **641**, 197.

[18] D. Serrate, J. M. Da. Teresa and M. R. Ibarra, Magnetoelastic coupling in $Sr_2(Fe_{1-x}Cr_x)ReO_6$ double perovskites, *J. Phys.: Condens. Matter.*, 2007, **19**, 436226.

[19] A. Nag, J. Manjanna, R. M. Tiwari and J. Gopalakrishnan, $Sr_4M_3ReO_{12}$ (M = Co, Fe): New ferromagnetic perovskite oxides, *Chem. Mater.*, 2008, **20**, 4420.

[20] W. Si, Y. Wang, Y. Peng and J. Li, Selective dissolution of *A*-site cations in ABO_3 perovskites: a new path to high-performance catalysts, *Angew. Chem. Int. Ed.*,2015, **54**, 7954.

[21] S. K. Pandey, R. Bindu, P. Bhatt, S.M. Chaudhari and A.V. Pimpale, Synthesis and investigation of structural and electronic properties of $Pr_{1-x}Ca_xFeO_3$ ($0 \leq x \leq 0.2$) compounds, *Physica B.*, 2005, **365**, 47.

[22] K.-I. Kobayashi, T. Kimura, H. Sawada, K. Terakuraand Y. Tokura, Room-temperature magnetoresistance in an oxide material with an ordered double-perovskite structure, *Nature*, 1998, **395**, 677-680.

[23] M.-R. Li, P. W. Stephens, M. Croft, Z. Deng, W. Li, C. Jin, M. Retuerto, J. P. Hodges, C. E. Frank, M. Wu, D. Walkerand M. Greenblatt, $Mn_2(Fe_{0.8}Mo_{0.2})MoO_6$: A double perovskite with multiple transition metal sub lattice magnetic effects, *Chem. Mater.*, 2018, **30**, 4508.

[24] S. Jaiswar and K. D. Mandal, Evidence of enhanced oxygen vacancies defects inducing ferromagnetism in multiferroic $CaMn_7O_{12}$ (CMO) manganite with sintering time, *J. Phys. Chem. C*, 2017, **121**, 19586.

[25] S. W. Kim, T. J. Emge, Z. Deng, R. Uppuluri, L. Collins, S. H. Lapidus, C. U. Segre, M. Croft, C.Jin, V. Gopalan, S. V. Kalinin and M. Greenblatt, $YCrWO_6$: Polar and magnetic oxide with $CaTa_2O_6$-related structure, *Chem. Mater.*, 2018, **30**, 1045.

[26] K. Dey, A. Indra, D. De, S. Majumdar and S. Giri, Magnetoelectric coupling, ferroelectricity, and magnetic memory effect in double perovskite $La_3Ni_2NbO_9$, *Appl. Mater. Interfaces*, 2016, **8**, 12901.

[27] M.-R. Li, J. P. Hodges, M. Retuerto, Z. Deng, P. W. Stephens, M. C. Croft, X. Deng, G. Kotliar, J. Sánchez-Benítez, D. Walker and M. Greenblatt, Mn_2MnReO_6: Synthesis and magnetic structure determination of a new transition-metal-only double perovskite canted antiferromagnet, *Chem. Mater.*, 2016, **28**, 3148.

[28] A. Hossain, P. Bandy Opadhyay and S. Roy, An overview of double perovskites $A_2B'B''O_6$ with small ions at A site: Synthesis, structure and magnetic properties, *J Alloy. Comp.*, 2018, **740**, 414.

[29] A. K. Paul, M. Reehuis, V. Ksenofontov, B. Yan, A. Hoser, D. M. Többens, P. M. Abdala, P. Adler, M. Jansen and C. Felser, Lattice instability and competing spin structures in the double perovskite insulator Sr_2FeOsO_6, *Phys. Rev. Lett.*, 2013, **111**, 167205.

[30] A. K. Paul, M. Jansen, B. Yan, C. Felser, M. Reehuis and P. M. Abdala, Synthesis, crystal structure, and physical properties of Sr_2FeOsO_6, *Inorg. Chem.*, 2013, **52**, 6713.

[31] R. C. Williams, F. Xiao, I. O. Thomas, S. J. Clark, T. Lancaster, G. A. Cornish, S. J. Blundell, W. Hayes, A. K. Paul, C. Felser and M. Jansen, Muon-spin relaxation study of the double perovskite insulators Sr_2BOsO_6 (B = Fe, Y, ln). *J. Phys.: Condens. Matter.*, 2016, **28**, 076001.

[32] A. K. Paul, M. Reehuis, C. Felser, P. M. Abdala and M. Jansen, Synthesis, crystal structure, and properties of the ordered double perovskite Sr_2CoOsO_6, *Z. Anorg. Allg. Chem.*, 2013, **639**, 2421.

[33] P. Adler, V. Ksenofontov, A. K. Paul, M. Reehuis, B. Yan, M. Jansen and C. Felser, Magnetic phase transitions and iron valence in the double perovskite Sr_2FeOsO_6, *Hyperfine Interact.*, 2014, **226**, 289.

[34] C. Felser and R. Seshadri, Conduction band polarization in some CMR materials: Evolving guidelines for new systems, *Int. J. Inorg. Mater.*, 2000, **2**, 677.

[35] A. Mamchik and I-W. Chen, Magnetic impurities in conducting oxides. I. $(Sr_{1-x}La_x)(Ru_{1-x}Fe_x)O_3$ system, *Phys. Rev. B*, 2004, **70**, 104409.

[36] A. Callaghan, C. W. Moellerand R. Ward, Magnetic interactions in ternary ruthenium oxides, *Inorg. Chem.*, 1966, **5**, 1572.

[37] K. Yoshimura, T. Imai, T. Kiyama, K. R. Thurber, A. W. Huntand K. Kosuge, ^{17}O-NMR Observation of universal behavior of ferromagnetic spin fluctuations in the itinerant magnetic system $Sr_{1-x}Ca_xRuO_3$, *Phys. Rev. Lett.*, 1999, **83**, 4397.

[38] R. J. Bouchard and J. F. Weiher, $La_{1-x}Sr_xRuO_3$: A new perovskite series, *J. Solid State Chem.*, 1972, **4**, 80.

[39] Y. Doi, Y. Hinatsu, A. Nakamura Y. Ishiib and Y. Morii, Magnetic and neutron diffraction studies on double perovskites A_2LnRuO_6 (*A* ~ Sr, Ba; *Ln* ~ Tm, Yb), *J. Mater. Chem.*, 2003, **13**, 1758.

[40] Y. Doi, Y. Hinatsu, K.-i. Oikawa, Y. Shimojoand Y. Morii, Magnetic and neutron diffraction study on the ordered perovskite Sr_2HoRuO_6, *J. Mater. Chem.*, 2000, **10**, 797.

[41] L. T. Corredor, D. A. L. Téllez, J. L. P. Jr, P. Pureurand J. Roa-Rojas, Magnetic, structural and morphological characterization of Sr_2GdRuO_6 double perovskite, *Int. J. Mod. Phys. A.*, 2011, **2**, 154.

[42] R. Sáez-Puche, E. Climent-Pascual, R. Ruiz-Bustos, M.A. Alario-Francoand M. T. Fernández-Díaz, Non-collinear magnetic structure of the Sr_2ErRuO_6 double perovskite, *Prog. Solid State Chem.*, 2007, **35**, 211.

[43] W. Xia, Q. Zhou, H. Xu, L. Chenand J. He, Magnetic and transport properties of the double perovskite Sr_2FeRuO_6, *Physica B*, 2008, **403**, 2189.

[44] P. M. Woodward, J. Goldberger, M. W. Stoltzfus, H. W. Eng, R. A. Ricciardo, P. N. Santhosh, P. KarenandA. R. Moodenbaugh, Electronic, magnetic, and structural properties of Sr_2MnRuO_6 and $LaSrMnRuO_6$ double perovskites, *J. Am. Ceram. Soc.*,2008, **91**, 1796.

[45] K.-W. Lee1 and W. E. Pickett, Half semi metallic antiferromagnetism in the $Sr_2Cr*T*O_6$ system (*T* = Os, Ru), *Phys. Rev. B*, 2008, **77**, 115101.

[46] K. Naveen, M. Reehuis, P. Adler, P. Pattison, A. Hoser, T. K. Mandal, U. Arjun, P. K. Mukharjee, R. Nath, C. Felser and A. K. Paul, Reentrant magnetism at the borderline between long-range antiferromagnetic order and spin-glass behavior in the *B*-site disordered perovskite system $Ca_{2-x}Sr_xFeRuO_6$, *Phys. Rev. B*, 2018, **98**, 224423.

[47] M. Fang, M. Kato, K. Yoshimura, and K. Kosuge, Magnetic and transport properties of the solid solution system $La_{1-x}Sr_xMnRuO_6$ with double perovskite structure, *J. Alloys. Comp*., 2001, **317**, 136.

[48] J-W. G. Bos and J. P. Attfield, Structural, magnetic, and transport properties of $(La_{1+x}Sr_{1-x})CoRuO_6$ double perovskites, *Chem. Matter.*, 2004, **16**, 1822.

[49] R. A. Ricciardo, H. L. Cuthbert, P. M. Woodward, Q. Zhou, B. J. Kennedy, Z. Zhang, M. Avdeev and L.-H. Jang, Structure and Properties of $Sr_{1-x}Ca_xMn_{0.5}Ru_{0.5}O_3$ Perovskites: Using Chemical Pressure to Control Mn/Ru Mixed Valency, *Chem. Mater*., 2010, **22**, 3369.

[50] H. L. Feng, M. P. Ghimire, Z. Hu, S.-C. Liao, S. Agrestini, J. Chen, Y. Yuan, Y. Matsushita, Y. Tsujimoto, Y. Katsuya, M. Tanaka, H.-J. Lin, C.-T. Chen, S.-C. Weng, M. Valvidares, K. Chen, F. Baudelet, A. Tanaka, M. Greenblatt, L. H. Tjeng and K. Yamaura, Room-temperature ferrimagnetism of antisite disordered Ca_2MnOsO_6, *Phys. Rev. Mater*., 2019, **3**, 124404.

[51] J. Rodríguez-Carvajal, Recent advances in magnetic structure determination by neutron powder diffraction, *Physica B*, 1993, **192**, 55.

[52] V. F. Sears, in *International Tables for Crystallography*, edited by A. J. C. Wilson (Kluwer Academic Publishers, Dordrecht/Boston/London, 1995), Vol. C, p. 383.

[53] A. K. Poswal, A. Agrawal, A. K. Yadav, C. Nayak, S. Basu, S. R. Kane, C. K. Garg, D. Bhattachryya, S. N. Jha and N. K. Sahoo, Commissioning and first results of scanning type EXAFS beamline (BL-09) at INDUS-2 synchrotron source, *AIP Conf. Proc.* 2014, **1591**, 649.

[54] S. Basu, C. Nayak, A. K. Yadav, A. Agrawal, A. K. Poswal, D. Bhattacharyya, S. N. Jha and N. K. Sahoo, A comprehensive facility for EXAFS measurements at the INDUS-2 synchrotron source at RRCAT, Indore, India, *J. Phys.: Conf. Ser.*, 2014, **493**, 012032.

[55] Z. Klencsár, A. Kuzmannand, and A. Vértes, User-friendly software for Mössbauer spectrum analysis, *J. Radioanal. Nucl. Chem.*, 1996, **210**, 105.

[56] R. I. Dass, J.-Q. Yanand, and J. B. Goodenough, Ruthenium doubles perovskite: Transport and Magnetic properties, *Phys. Rev. B*, 2004, **69**, 094416.

[57] A. Sinclair, J. A. Rodgers, C. V. Topping, M. Msek, R. D. Stewart, W. Kockelmann, J.-W. G. Bos and J. P. Attfield, Synthesis and Properties of Lanthanide Ruthenium (III) Oxide Perovskites, *Angew. Chem. Int. Ed.*, 2014, **53**, 8343.

[58] T. Vitova, S. Mangold, C. Paulmann, M. Gospodinov, V. Marinova, and B. Mihailova, X-ray absorption spectroscopy of Ru-doped relax or ferroelectrics with a perovskite-type structure, *Phys. Rev. B*, 2014, **89**, 144112.

[59] *X-Ray Absorption: Principles, Applications, Techniques of EXAFS, SEXAFS and XANES*, edited by D.C. Konigsberger and R. Prince, EXAFS in Catalysis Instrumentation and Applications, (Wiley, New York, 1988).

[60] H. Nakatsugawa, E. Iguchi, and Y. Oohara, Electronic structures and magnetic properties in $Sr_{1-x}La_xRuO_3$ ($0.0 \leq x \leq 0.5$), *J. Phys. Condens. Matter.*, 2002, **14**, 415.

[61] E. F. Bertaut, *Acta Cryst. A*, 1968, **24**, 217.

[62] M. Reehuis, C. Ulrich, P. Pattison, B. Ouladdiaf, M. C. Rheinstädter, M. Ohl, L. P. Regnault, M. Miyasaka, Y. Tokura, and B. Keimer, Neutron diffraction study of YVO_3, $NdVO_3$, and $TbVO_3$, *Phys. Rev. B*, 2006, **73**, 094440.

[63] M. Schmidt, M. Hofmann andS. J. Campbell, Magnetic structure of strontium ferrite $Sr_4Fe_4O_{11}$, *J. Phys. Condens. Matter*, 2003, **15**, 8691.

[64] P. M. Woodward, D. E. Cox, E. Moshopoulou, A. W. Sleightand S. Morimoto, Structural studies of charge disproportionation and magnetic order in $CaFeO_3$,*Phys. Rev. B*, 2000, **62**, 844.

[65] F. M. D. Costa, R. Greatrex and N. N. Greenwood, A study of the perovskite solid solution series $La_xSr_{1-x}RuO_3$ and $La_xCa_{1-x}RuO_3$, by ruthenium-99 Mössbauer spectroscopy, *J. Solid State Chem.*, 1977, **20**, 381.

[66] G. Popov, M. Greenblatt, and M. Croft, Large effects of *A*-site average cation size on the properties of the double perovskites $Ba_{2-x}Sr_xMnReO_6$: A d^5-d^1 system, *Phys. Rev. B*, 2003, **67**, 024406.

[67] L. Zhang and Z. J. Tang, Polaron relaxation and variable-range-hopping conductivity in the giant-dielectric-constant material $CaCu_3Ti_4O_{12}$, *Phys. Rev. B*, 2004, **70**, 174306.

[68] S. K. Deshpande, S. N. Achary, R. Mani, J. Gopalakrishnan and A. K. Tyagi, Low-temperature polaronic relaxations with variable range hopping conductivity in $FeTiMO_6$ (*M* = Ta, Nb, Sb), *Phys. Rev. B*, 2011, **84**, 064301.

Table 1. Results of the crystal structure refinements of $Ca_{1.5}La_{0.5}FeRuO_6$, $CaLaFeRuO_6$ and La_2FeRuO_6 obtained from x-ray and neutron powder data. For the sake of completeness, the data of Ca_2FeRuO_6, given in Ref. [46], are also presented. The refinements of the data sets were carried out in the orthorhombic space group *Pbnm*, where both Fe and Ru statistically occupy the Wyckoff position 4*b*(½,0,0). The Ca and O1 atoms are located at the Wyckoff position 4*c*(*x*,*y*,¼), while the O2 atoms are located at the position 8*d*(*x*,*y*,*z*). The residual R_F is defined as $R_F = \sum||F_{obs}| - |F_{calc}||/\sum|F_{obs}|$). The equatorial ($d_{eq}$) and apical bond lengths (d_{ap}), the averaged bond lengths (d_{av}) of the TO_6 octahedra (*T* = Fe, Ru) as well as Bond Valence Sum (BVS) are also listed. The bond distances are given for the atoms located at the following positions:*B* in (0,½,0), O2 in (*x*–1,*y*,*z*), O2′ in (*x*–½,½–*y*,–*z*).

	Ca_2FeRuO_6		$Ca_{1.5}La_{0.5}FeRuO_6$		$CaLaFeRuO_6$		La_2FeRuO_6	
T [K] / radiation	298 / x-ray	3 / neutron	298 / x-ray	3 / neutron	298 / x-ray	3 / neutron	298 / x-ray	3 / neutron
a [Å]	5.3995 (3)	5.3849(4)	5.4421(3)	5.4253(5)	5.4845(3)	5.4713(5)	5.5706(1)	5.5672(6)
b [Å]	5.4756 (3)	5.4703(5)	5.5112(3)	5.5096(6)	5.5369(3)	5.5354(5)	5.5893(1)	5.5913(6)
c [Å]	7.6714(4)	7.6520(6)	7.7278(4)	7.7124(8)	7.7806(3)	7.7666(7)	7.8764(2)	7.8698(8)
V [Å^3]	226.81(2)	225.40(3)	231.78(2)	230.53(4)	236.27(2)	235.22(4)	245.24(1)	244.97(4)
x(Ca/La)	0.9942(13)	0.9876(13)	0.9939 (8)	0.9889(13)	0.9945 (6)	0.9889(13)	0.9962(6)	0.9923(14)
y(Ca/La)	0.0431(5)	0.0424(5)	0.0366(3)	0.0406(5)	0.03468(19)	0.0392(5)	0.0433(3)	0.0362(5)
x(O1)	0.066 (2)	0.0845(7)	0.0751(18)	0.0802(10)	0.0689(20)	0.0808(11)	0.064(2)	0.0717(14)
y(O1)	0.4790 (18)	0.4768(6)	0.4840(14)	0.4800(9)	0.4805(11)	0.4799(10)	0.4978(14)	0.4852(11)
x(O2)	0.7009 (20)	0.7080(4)	0.7153(18)	0.7060(7)	0.7107(12)	0.7073(7)	0.7128(16)	0.7170(8)
y(O2)	0.2962 (18)	0.2953(4)	0.2815(15)	0.2918(6)	0.2878 (11)	0.2907(7)	0.278 (2)	0.2874(8)
z(O1)	0.0465 (10)	0.0432(3)	0.0477(9)	0.0421(5)	0.0449(9)	0.0426(5)	0.0452(10)	0.0443(6)
B(Ca/La) [Å^2]	0.63 (7)	0.51(5)	0.77 (6)	0.40(5)	0.61 (6)	0.37(5)	0.52 (3)	0.52(5)
B(O1) [Å^2]	0.47 (4)	0.26(2)	0.54 (9)	0.29(3)	2.74 (4)	0.29(3)	0.87 (12)	0.27(3)
B(O2) [Å^2]	0.31 (2)	0.45(2)	0.81 (10)	0.47(3)	0.94 (7)	0.63(3)	0.63 (5)	0.64(4)
R_F	0.0195	0.0256	0.0141	0.0340	0.0156	0.0371	0.0262	0.0337
$d_{1,eq}$(*B*-O2) [Å]	1.995(10)	1.957(2)	1.996(7)	1.991(3)	2.005(6)	2.004(4)	2.054(9)	2.004(5)
$d_{2,eq}$(*B*-O2′) [Å]	1.983(10)	1.991(2)	1.978(7)	1.985(3)	1.999(6)	1.996(4)	1.986(10)	2.040(5)
$d_{3,ap}$(*B*-O1) [Å]	1.954(2)	1.968(9)	1.976(2)	1.980(1)	1.984(2)	1.994(1)	2.002(2)	2.009(2)
d_{av}(*B*-O) [Å]	1.977(3)	1.972(2)	1.983(6)	1.985(8)	1.995(6)	1.998(9)	2.014(3)	2.018(11)
∠(*B*-O1-*B*) [°]	150.2(5)	152.3(2)	153.8(3)	153.8(3)	153.3(3)	153.6(3)	157.8(1)	156.6(4)
∠(*B*-O2-*B*) [°]	153.2(2)	152.4(2)	154.8(3)	153.2(2)	155.5(1)	154.6(2)	159.4(1)	157.1(1)
BVS								
Fe	3.32		3.26		3.15		3.03	
Ru	4.86		4.77		3.84		3.61	

Table 2. Oxidation state of Ru in reference materials and the energy shift of the Ru-K edge with respect to that of metal Ru.

Sample	ΔE	Oxidation state
Ru metal	0 ± 0.21	0
$RuCl_3$	8.42 ± 0.12	3
RuO_2	13.39 ± 0.28	4
$SrRuO_3$	12.98 ± 0.39	4
Ca_2FeRuO_6	14.60 ± 0.16	5
$Ca_{1.5}La_{0.5}FeRuO_6$	13.25 ± 0.15	4.32*
$CaLaFeRuO_6$	12.42 ± 0.17	4.01*
La_2FeRuO_6	11.46 ± 0.28	3.68*

* Calculated oxidation states using linear function.

Table 3. Local structural parameters obtained from the EXAFS fitting.

Path	Parameter	Ca_2FeRuO_6	$Ca_{1.5}La_{0.5}FeRuO_6$	$CaLaFeRuO_6$	La_2FeRuO_6
Ru-O	R (Å)	1.96 ± 0.01	1.97 ± 0.01	1.99 ± 0.01	2.02 ± 0.01
	N	5.99 ± 0.25	5.90 ± 0.53	5.09 ± 0.81	5.32 ± 0.49
	σ^2	0.0043 ± 0.0013	0.0045 ± 0.0008	0.0025 ± 0.0015	0.0057 ± 0.0012

Table 4. Observed ordering temperature for the three compounds. T_m represents the onset temperature for magnetic ordering from NPD data and $T_{m'}$ represents the maxima in the ZFC dc magnetic measurement.

Compounds	T_m(K)	$T_{m'}$(K)
$Ca_{1.5}La_{0.5}FeRuO_6$	275	120
$CaLaFeRuO_6$	435	170
La_2FeRuO_6	570	300

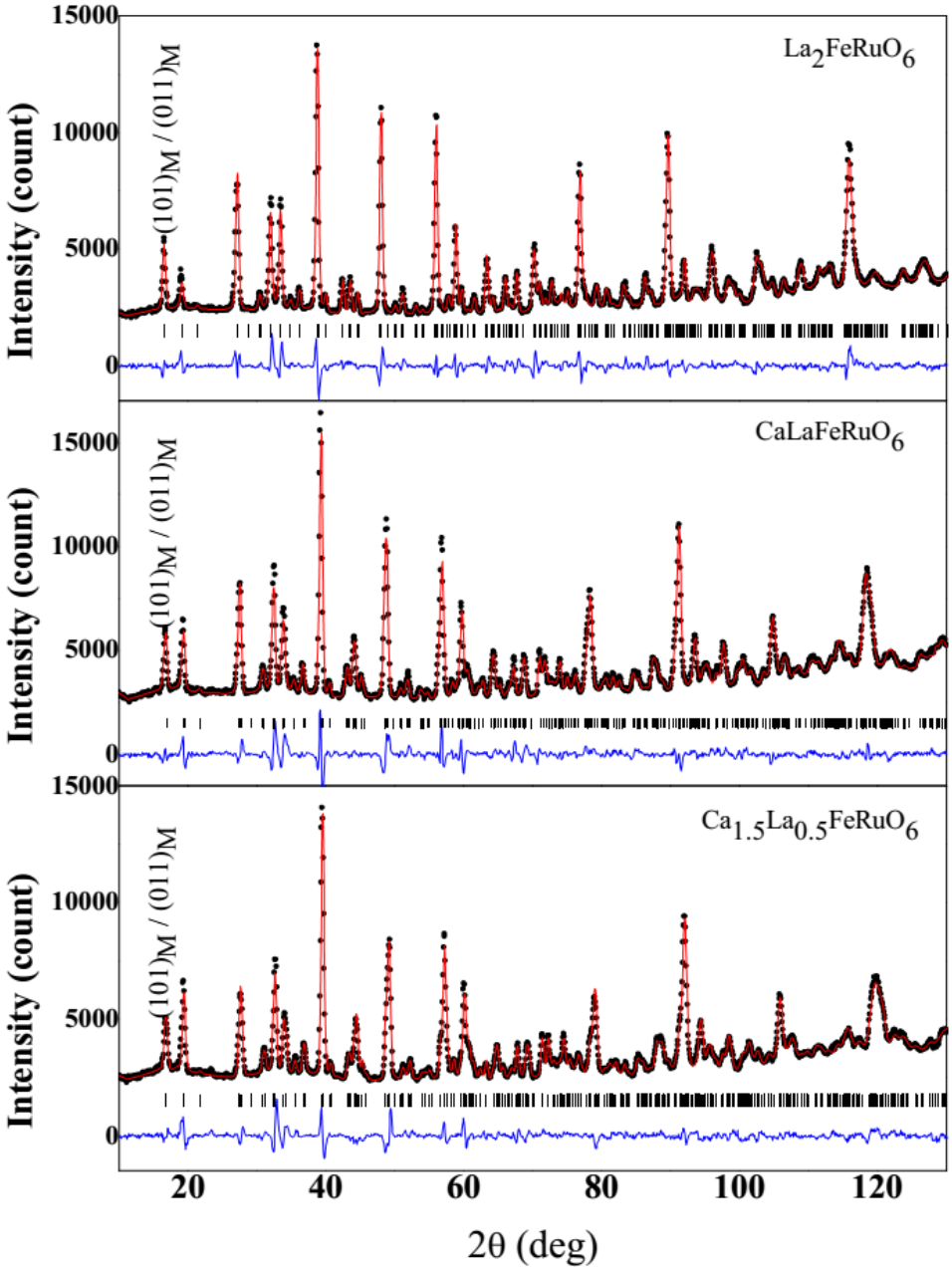

Fig. 1. Results of the Rietveld refinements of the neutron powder diffraction data of $Ca_{1.5}La_{0.5}FeRuO_6$, $CaLaFeRuO_6$ and La_2FeRuO_6 collected 3 K on the instrument E9 (λ = 1.309 Å). The crystal structure of these compounds was refined in the orthorhombic space group *Pbnm*. The calculated patterns (red) are compared with the observed ones (black circles). The difference patterns (blue) as well as the positions (black bars) of the nuclear Bragg reflections are also shown. The reflection pair 101/011 is of almost purely magnetic origin for all compounds. No satisfactory peak-profile refinements could be obtained for all samples using a Pseudo-Voigt function. This may be ascribed to the presence of strain effects and inhomogeneities in the disordered powder samples. The fit could not be improved by using different strain-size models.

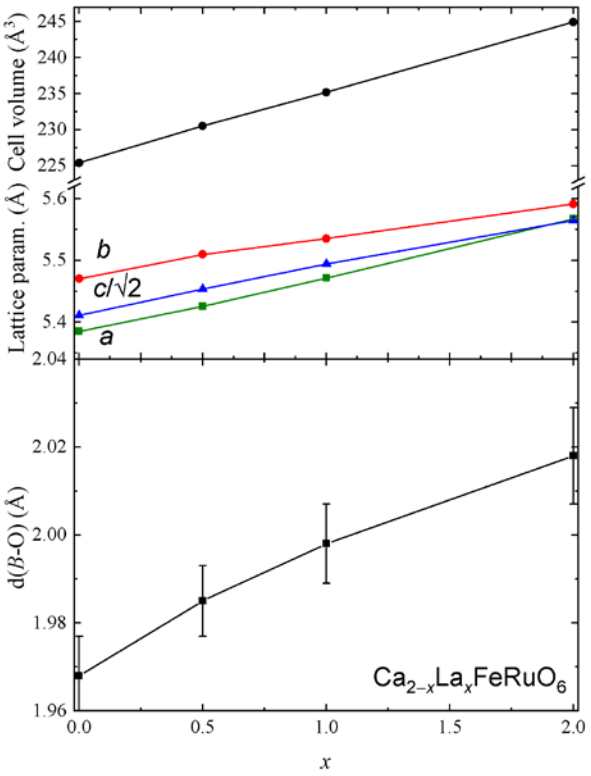

Fig. 2.Variation of the lattice parameters in the system $Ca_{2-x}La_xFeRuO_6$ at 3 K as determined from neutron diffraction data. In the lower part of the figure, the change of average bond lengths *d*(*B*-O) in the BO_6 octahedra (*B* = Fe, Ru) is shown. The transition metal site, located at the Wyckoff position 4*b*, is statistically occupied with Fe and Ru atoms.

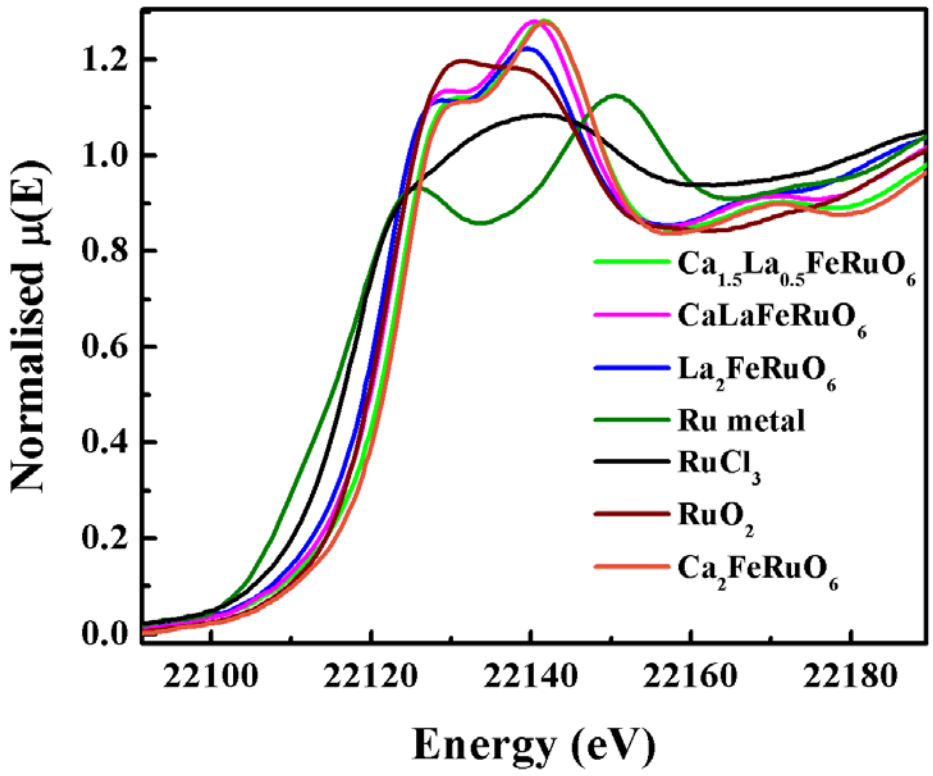

Fig. 3. Normalised XANES spectra at the Ru-K edge for all three compounds along with reference spectra.

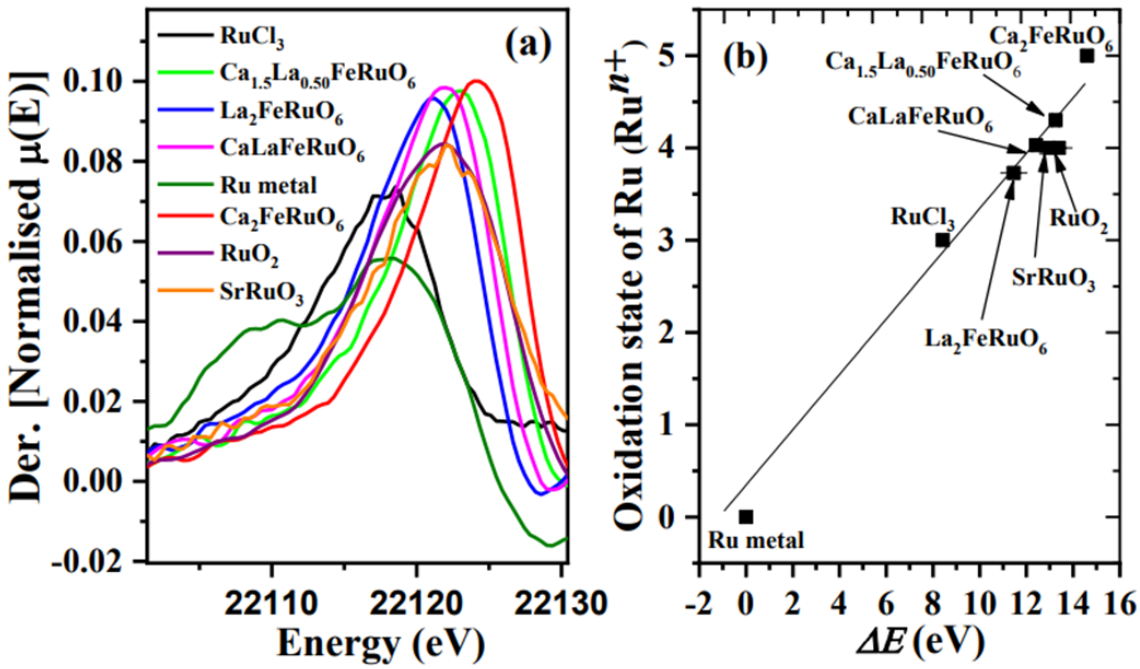

Fig. 4. (a) Derivative spectra of normalised XANES and (b) oxidation state of Ru in reference materials *Vs* the shift of the Ru-K edge with respect to that of metal Ru. The solid line represents a linear fit to the data points of reference materials.

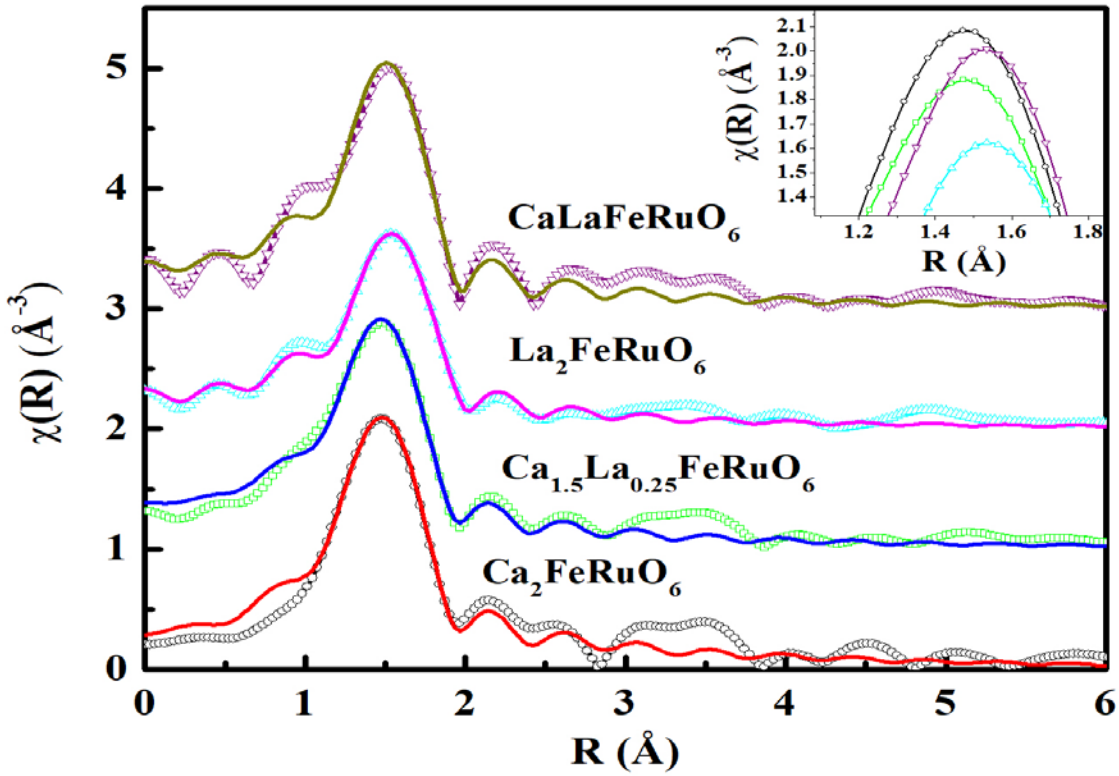

Fig. 5. Fourier transformed EXAFS spectra at Ru-K edge. The experimental spectrum is represented by Scatter points and theoretical fit is represented by Solid line. The spectrum is vertically shifted for better representation. The inset shows the enlarge view of first coordination peak without vertical shift.

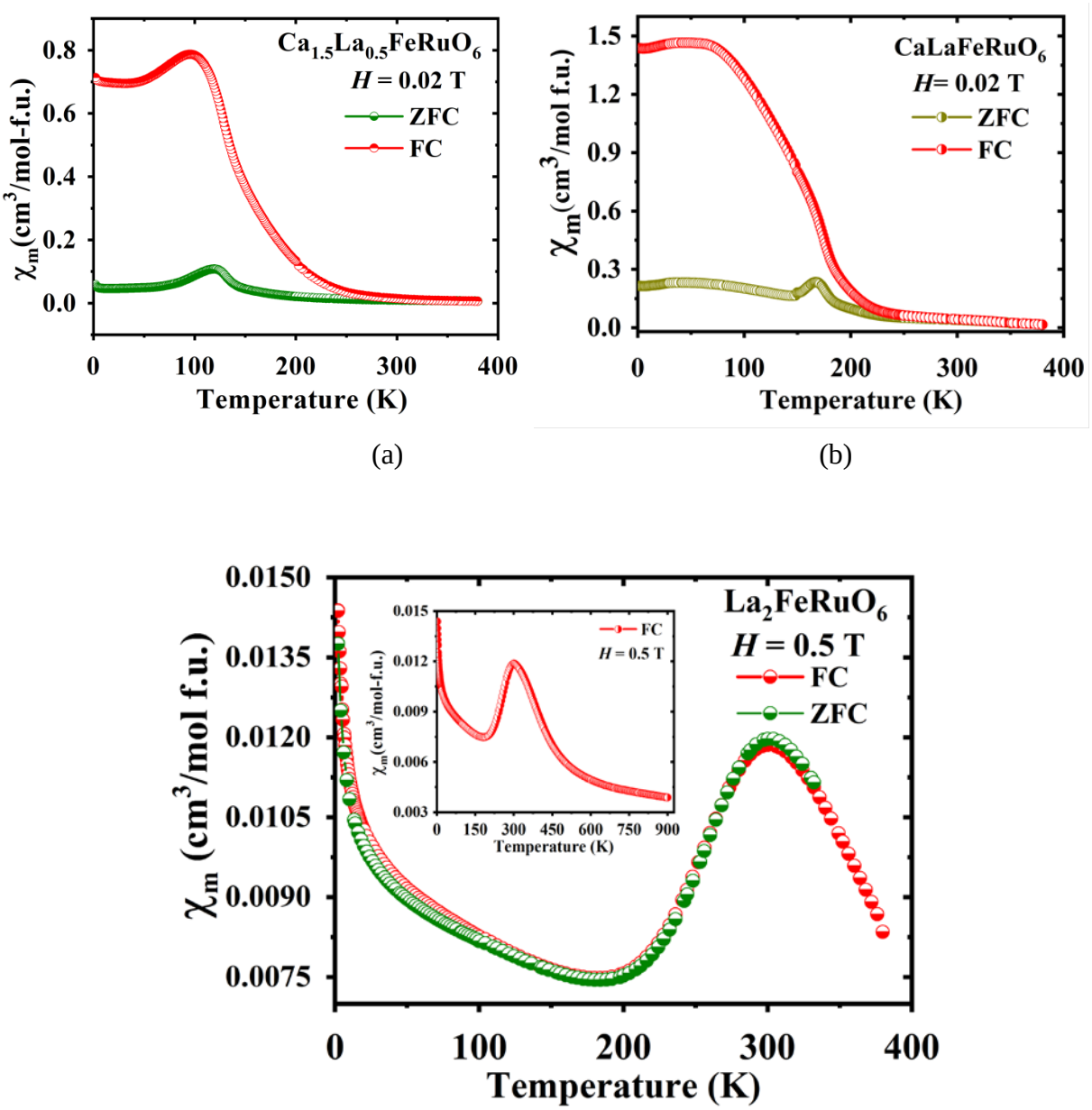

Fig. 6. ZFC and FC susceptibilities vs *T* measured for (a) $Ca_{1.5}La_{0.5}FeRuO_6$, (b) $CaLaFeRuO_6$, and (c) La_2FeRuO_6. Note that the high temperature FC susceptibility is also measured for finding any possible secondary transition of La_2FeRuO_6 (Inset of Figure c).

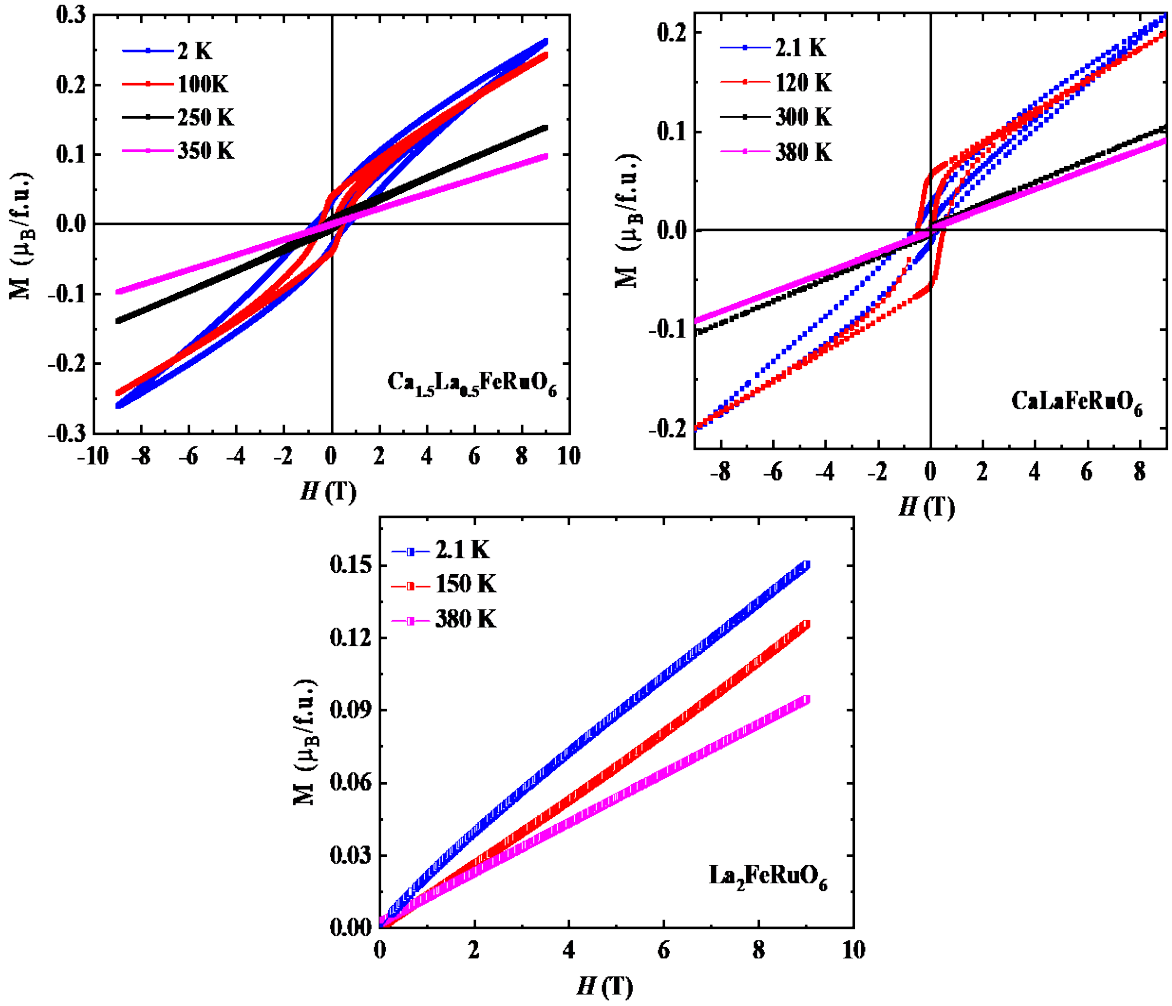

Fig. 7. Isothermal magnetization (*M* vs *H*) measured at different temperatures for $Ca_{1.5}La_{0.5}FeRuO_6$, $CaLaFeRuO_6$ and La_2FeRuO_6.

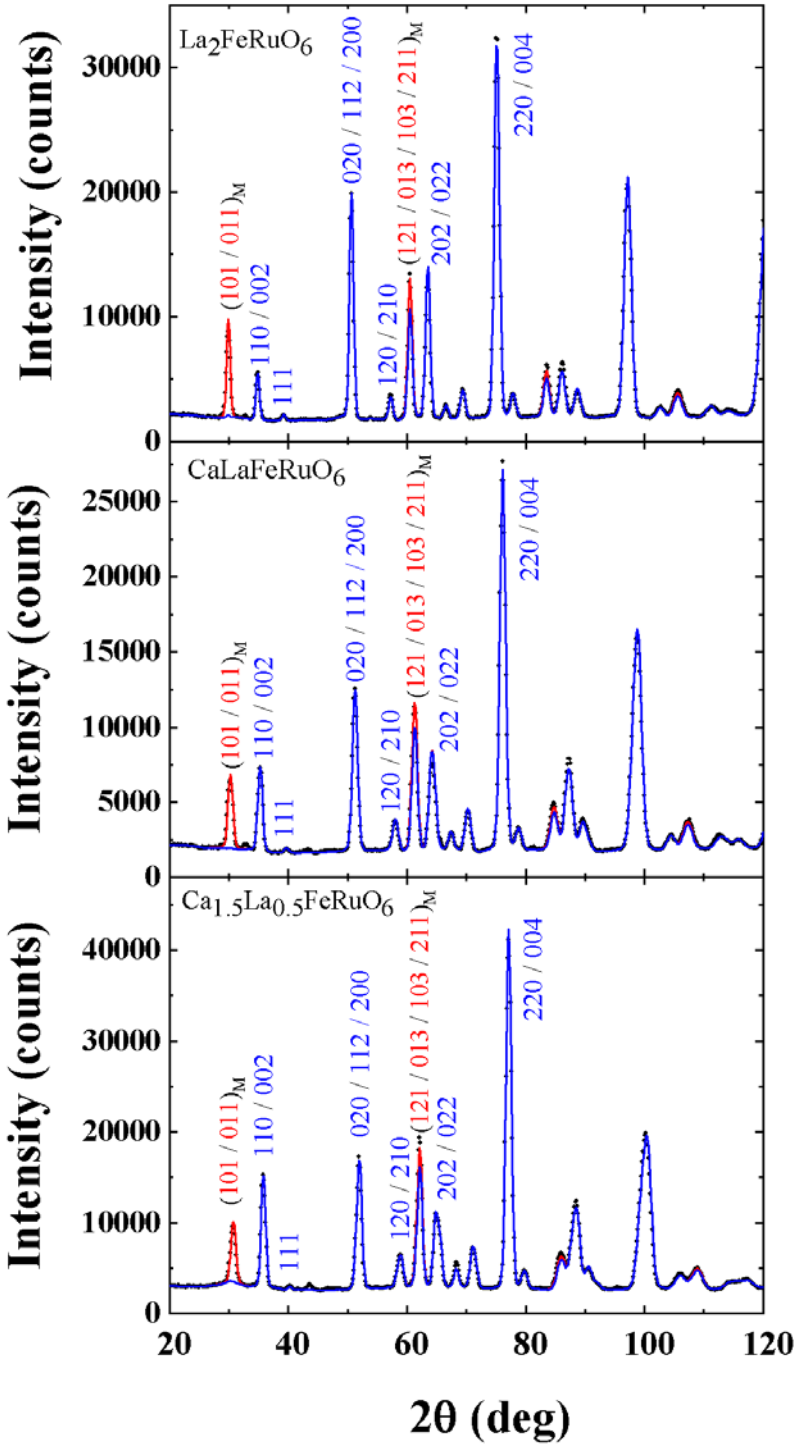
La2FeRuO6
CaLaFeRuO6
Ca1.5La0.5FeRuO6
Intensity (counts)
2θ (deg)
(101 / 011)M
110 / 002
111
020 / 112 / 200
120 / 210
(121 / 013 / 103 / 211)M
202 / 022
220 / 004

Fig. 8. Neutron powder patterns of $Ca_{2-x}La_xFeRuO_6$ (x = 0.5, 1.0, and 2.0) taken on instrument E6 (λ = 2.43 Å) at 3 K. The calculated patterns of the pure nuclear contribution (blue) as well as the sum of the nuclear and the magnetic contributions (red) are compared with the observed ones (black circles). The strongest magnetic intensity appears at the positions of the reflection pair 101 and 011 indicating the presence of a *G*-type spin ordering.

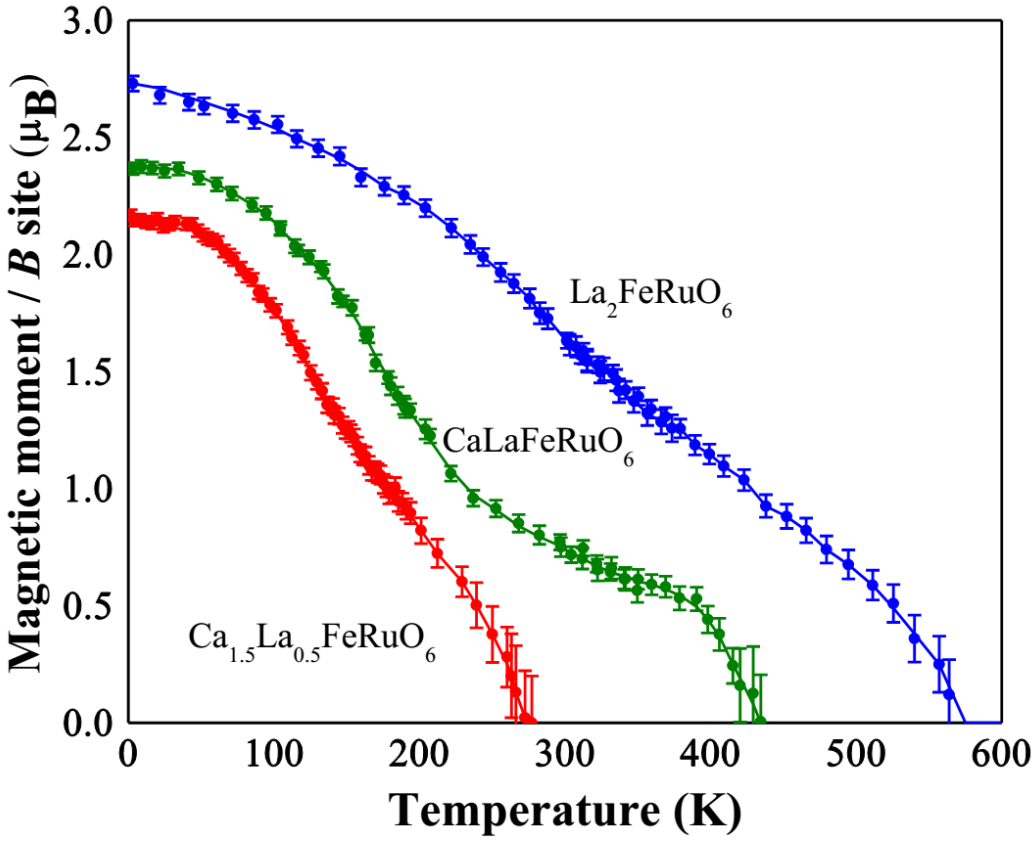

Fig. 9. Temperature dependence of the average magnetic moments of the *B*-site atoms at the Wyckoff position 4*b* which is statistically occupied with Fe and Ru atoms. Long-range magnetic ordering sets in at 275 K ($Ca_{1.5}La_{0.5}FeRuO_6$), 435 K ($CaLaFeRuO_6$), and 570 K (La_2FeRuO_6), respectively.

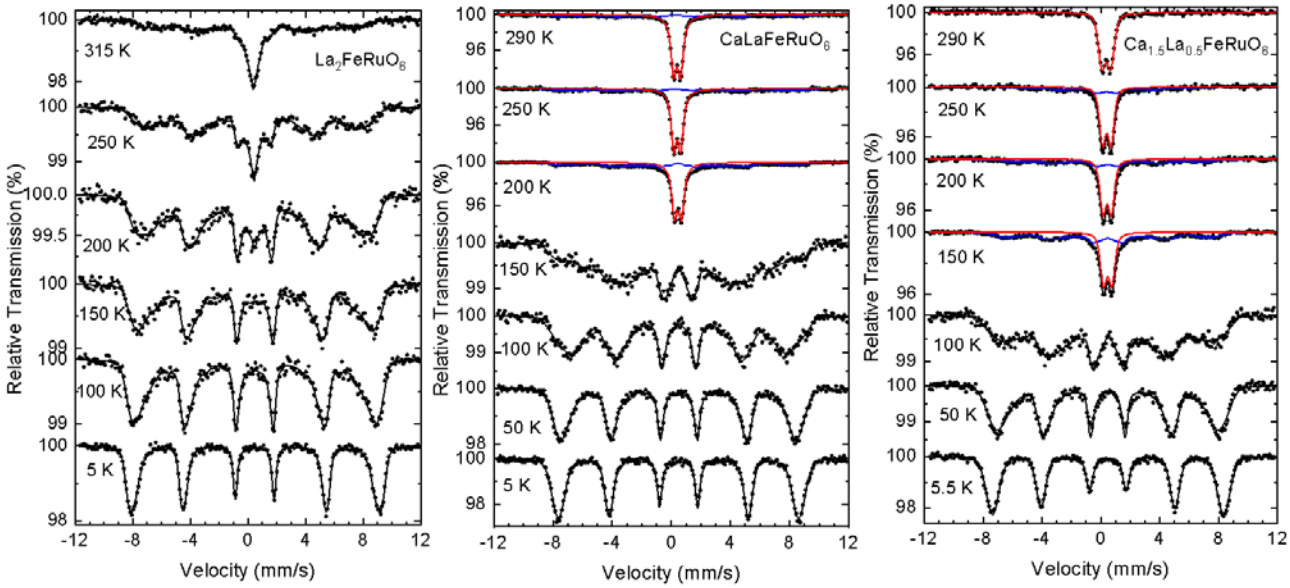

Fig. 10. ^{57}Fe Mössbauer spectra of the three compounds measured at the indicated temperatures. Dots correspond to the experimental data, full lines to the calculated spectra and subspectra. Note that iron is in the Fe^{3+} state for all the three compounds.

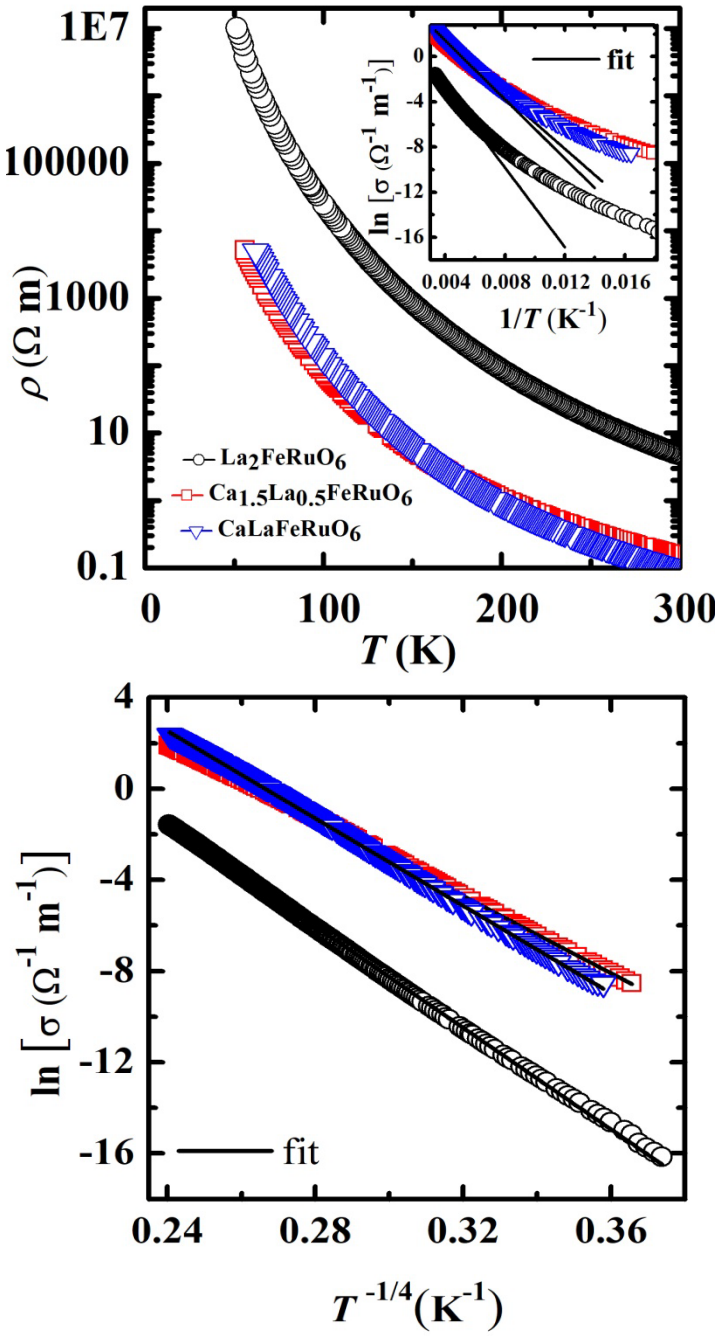

Fig. 11. Upper panel: Temperaturedependent electrical resistivity (ρ) of $Ca_{1.5}La_{0.5}FeRuO_6$, $CaLaFeRuO_6$, and. La_2FeRuO_6, Inset: ln σ vs $1/T$ plot for all the three compounds. The solid lines are the linear fits using Eq. (3). Lower panel: ln σ vs $T^{-1/4}$ plots for $Ca_{1.5}La_{0.}5FeRuO_6$, $CaLaFeRuO_6$, and La_2FeRuO_6. The solid lines are the linear fits assuming that the conductivity obeys the VRH transport mechanism.